Nonlinear photonic crystals with two-dimensional quasi-periodic and fractal superlattices

Boqin Ma (马博琴)[1*], Mingliang Ren (任明亮)[2], and Zhiyuan Li (李志远)[2]

[1] *College of Science, Communication University of China, Beijing 100024, China*

[2] *Institute of Physics, Chinese Academy of Sciences, Beijing 100190, China*

[*] *Corresponding author: maboqin@cuc.edu.cn*

Received May 25, 2012; accepted June 25, 2012; posted online December 5, 2012

High quality z-cut $LiNbO_3$ nonlinear photonic crystals with two-dimensional (2D) dodecagonal and fractal superlattices are successfully fabricated by applying the high voltage pulses. By collinear quasi-phase matching technique, second-harmonics at five wavelengths and ten wavelengths are observed simultaneously in one poled crystal, respectively. The same results can be obtained by rotating around the z axis by integrals of 30° in quasi-periodically poled crystal. In fractal nonlinear photonic crystal, the normalized conversion efficiency can be as high as 0.53%/mW for 499-nm second-harmonic laser spot.

OCIS codes: 190.4223, 140.3515.

doi: 10.3788/COL201210.S21904.

The concept of quasi-phase matching (QPM), proposed by Armstrong in 1962, means that phase velocity mismatching in nonlinear interactions can be compensated by using the exact reciprocal vectors[1]. During the QPM interactions in nonlinear photonic crystal (NPC), reciprocal vectors (RVs) $\overrightarrow{G}$ can compensate the mismatching of wave vectors $\Delta\overrightarrow{K} = \overrightarrow{K}_2 - 2\overrightarrow{K}_1$, in which $\overrightarrow{K}_1$ and $\overrightarrow{K}_2$ are the wave vectors of the fundamental and the second-harmonic beams. QPM technique was not widely applied in nonlinear frequency conversion until NPC was successfully fabricated by electric field poling technique. Previously, the conception of QPM mainly focused on one-dimensional (1D) structures, such as periodic and Fibonacci quasi-periodic structures[2,3]. Then, more and more researchers paid more attentions to QPM harmonics and optical parametric oscillator (OPO). And the domain structures of NPC were gradually extended to two-dimensional (2D) plane, and even three-dimensional (3D) space[4,5]. Many new optical properties in NPC have been explored, such as the linear polarization-state generator, the Ĉerenkov second-harmonic generation, the surface acoustic waves generation, and femtosecond laser-written waveguides, etc.[6−9]. In this letter, the nonlinear photonic crystals with 2D dodecagonal and H fractal superlattices were fabricated. The collinear QPM second harmonic generations of multiple-wavelengths were explored in one piece of NPC.

The dodecagonal structures can be formed by using Stampfli inflation system for the basic square-triangle tiling unit (side length d)[10]. Firstly, form the parent square-triangle tiling by 6 squares and 12 triangles, whose side lengths are $(2+\sqrt{3})d$. Next, place regular dodecagons on the big parent square-triangle tiling, with their centers lying at the vertices of the tiling and their sides running perpendicular to tiling edges; then erase the big parent square-triangle tiling. Finally, tile each dodecagon (sixfold-symmetric) with 6 squares and 12 triangles in one way. Then the initial 12-fold structure is accomplished as illustrated in Fig. 1(a). The H-shaped fractal can be formed by thousands of 3-μm-thick lines of length a_l. The first level is constructed of a line of length a_1=1 024 μm, then two lines (length a_2=1 024 μm) as the second level are drawn at right angles and connected to the end of the first level at their midpoints. The third and fourth levels are constructed similarly except the line length is scaled down by a factor of 2 (a_3 and a_4=512 μm). By continuing this procedure, a self-similar H fractal structure is realized in a two-dimensional plane as shown in Fig. 1(b).

A He–Ne laser beam was incident normally on the poled NPC. The diffraction light field of the dodecagonal and fractal superlattices was recorded by a digital camera, as shown in Fig. 2. The diffraction pattern actually resembles the Fourier transform of the real space lattice. The locations of the diffractive spots correspond to the ones of RVs that can be used for QPM nonlinear interactions, and the size of the spots indicates the size of the corresponding Fourier coefficients. As shown in Fig. 2(a), it is seen clearly that the diffraction pattern displays 12-fold rotational symmetry in reciprocal space, which is greatly similar to the real space. Moreover, laser beam was incident normally on the fractal NPC. As shown in Fig. 2(b), it is obvious that the diffraction pattern is self-similar (not periodic) with a 1/2 scaling factor, particularly near the optical center. The intensity distribution is different in horizontal and vertical directions, which is caused by anisotropy of the H fractal of finite levels. The H fractal structure has the following features. Firstly, the diffraction pattern is consistent under scaling. Secondly, some diffracted spots become even brighter when moving

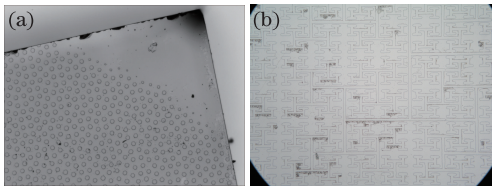

Fig. 1. Optical micrographs of the etched 2D poled $LiNbO_3$ NPC at $+z$ surface. (a) Dodecagonal superlattice; (b) fractal superlattice.

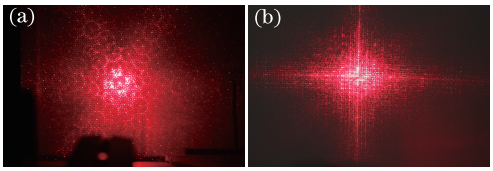

Fig. 2. Diffraction pattern: (a) 2D dodecagonal superlattice structure; (b) H-shape fractal superlattice.

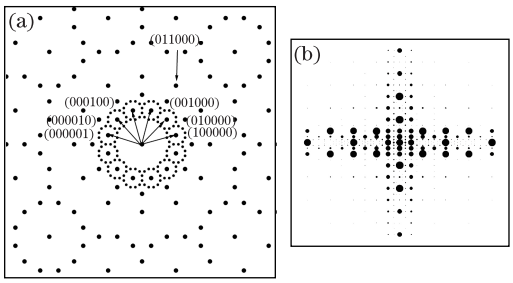

Fig. 3. Reciprocal vectors: (a) 12-fold superlattice structure; (b) H fractal structure.

away from the center. These lead to plenty of reciprocal vectors existing in H fractal reciprocal space, which exactly provide the possibility of multiple wavelength frequency conversions in a $LiNbO_3$ NPC with H fractal superlattice. For the first feature, a multiple of the shorter reciprocal vectors can form the combined longer ones. For the second feature, the longer reciprocal vectors can be gotten directly. As illustrated in Figs. 3(a) and (b), the reciprocal spaces of dodecagonal and fractal structures were given.

Considering $\overrightarrow{k}_2 = 2\overrightarrow{k}_1 + \overrightarrow{G}$ in second-harmonic generation, collinear quasi-phase matching processes of different wavelengths can be realized simultaneously. During perfect QPM interactions, phase mismatching $\Delta\overrightarrow{k} = \overrightarrow{k}_2 - 2\overrightarrow{k}_1 - \overrightarrow{G}$ is zero. In this letter, the collinear QPM second-harmonic interactions are mainly considered, which means that the fundamental and harmonic wave vectors and the used reciprocal vectors are collinear. The collinear QPM second-harmonic interactions were carried out under a tunable nanosecond OPO pumped by a Nd:YAG laser, whose repetition rate and pulse width were 10 Hz and 4 ns, respectively. The laser beams were perpendicularly incident on the $LiNbO_3$ NPC with 12-fold superlattice and parallel to the reciprocal vector (001100). Within the allowable range of the OPO laser beams, five second-harmonics at 620, 574, 555, 515, and 492 nm were clearly observed, as shown in Fig. 4. Series of line-shaped patterns at their symmetric positions may result from non-collinear QPM interactions. With the fundamental or harmonic wavelengths decreasing, the reciprocal vectors increase gradually. The RVs at 620, 574, 555, 515, and 492 nm are 0.584, 0.731, 0.81, 1.024, and 1.188 μm^{-1} respectively. The RV $\overrightarrow{G}_1$ for 620 nm is due to the long diagonal lines of rhombi a, which is the most common RV, or the sum of the short diagonal lines of rhombi b and the diagonal lines of squares c, i.e. $(b+c)$. For example, $\overrightarrow{G}_1$ corresponds to (001100) or (010010)+(100001). The RV $\overrightarrow{G}_2$ for 574 nm is due to the sum of the long diagonal lines of rhombi a and the short diagonal lines of rhombi b i.e. $(a+b)$ or the sum of twice the short diagonal lines of rhombi $2b$ and the diagonal lines of squares c i.e. $(2b+c)$. The RV $\overrightarrow{G}_3$ for 555 nm may be due to $2c$ and $a+2b$. The RV $\overrightarrow{G}_4$ for 515 nm is due to $b+2c$ or $a+c$. The RV $\overrightarrow{G}_5$ for 492 nm is due to three kinds of allowable combination $2a$, $a+b+c$, or $2b+2c$. We calculate that $\overrightarrow{G}_1 : \overrightarrow{G}_2 : \overrightarrow{G}_4 : \overrightarrow{G}_5$ is 1:1.26:1.73:2, which agrees well with the ratio above. But for 555 nm, $\overrightarrow{G}_1 : \overrightarrow{G}_3$ is 1:1.46 for $(2c)$ and 1:1.53 for $(a+2b)$. With contrast with the ration 1:1.38 above, the difference is very obvious. At second-harmonic wavelengths of 620, 492, and 555 nm, the conversion efficiencies were 6.69%, 1.38%, and 0.44%, the input powers were 3.6, 4.7, and 5.5 mW, respectively. The normalized conversion efficiency was the maximum for 620 nm, but the minimum for 555 nm. These may result from the most possible distribution of the RV for 620 nm harmonic output, which equals the long diagonal lines of rhombi. And considering the ratio with larger difference, worse harmonic pattern in Fig. 4(c) and lower conversion efficiency comprehensively, the 555-nm harmonics may attribute to the phase

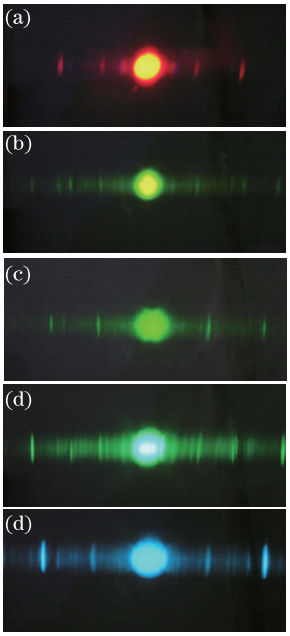

Fig. 4. Five collinear QPM second harmonics in $LiNbO_3$ NPC with 12-fold superlattice. (a) 620, (b) 574, (c) 555, (d) 515, and (e) 492 nm.

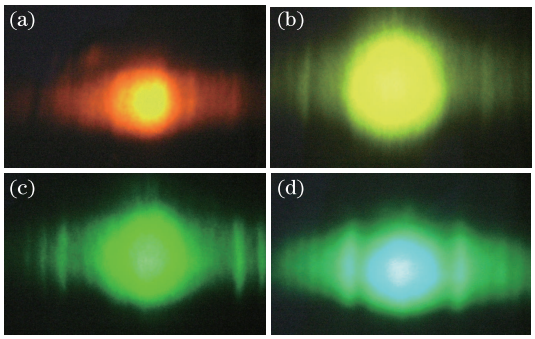

Fig. 5. (Color online) Second-harmonic spots under nanosecond laser beams as the input fundamental waves. Wavelengths and colors of harmonic spots are (a) 592 (orange), (b) 577 (yellow), (c) 544 (green), and (d) 517 nm (blue-green), respectively.

mismatching in QPM processes by using RVs relating to $2c$ and $a+2b$. The higher normalized conversion efficiency for 492 nm may be due to the RV $\overrightarrow{G}_5$ of three combination modes.

In the fractal reciprocal space, eight kinds of second-harmonics were realized, which mainly attributed to plenty of reciprocal vectors. Figure 5 partly shows the harmonic patterns of 592 (orange), 577 (yellow), 544 (green), and 517 nm (blue-green). It could be concluded that the conversion efficiencies at the short and long wavelengths were higher than that at the mid-wavelengths. For example, the fine harmonic pattern at wavelength 577 nm was obtained, and the conversion efficiency was 1.7% when the input power was 5.3 mW. However, for 499 nm second-harmonic output, the normalized conversion efficiency was 0.53%/mW, which might be due to longer RVs based on the diffraction analysis as explained above. And for 674-nm second-harmonic output, the normalized conversion efficiency was 0.42%/mW, which related to the low-order reciprocal vectors. In QPM processes, more effective harmonics can be achieved for lower-order reciprocal vectors. Generally, the normalized conversion efficiencies were less than 1%/mW under different wavelengths, which was due to the higher-order reciprocal vectors. Because the lower-order reciprocal vectors were too short to satisfy the QPM second-harmonic processes within the allowable range of OPO laser beams.

In conclusion, by quasi-phase matching technique, five harmonic processes are accomplished simultaneously in one poled $LiNbO_3$ crystal with 2D dodecagonal quasi-periodic superlattice. At second-harmonic wavelength of 620 nm, the normalized conversion efficiency is 1.9%/mW and the corresponding RV can be (001100). The similar results can be obtained 12 times by rotating this crystal around the z axis by integrals of 30°. Moreover, the $LiNbO_3$ nonlinear photonic crystal with H fractal superlattice is successfully prepared. More than ten harmonic wavelengths, including red, yellow, green, and blue, are obtained along two mutually perpendicular directions in one crystal. For the input fundamental wavelength at 998 nm, the normalized conversion efficiency could reach 0.53%/mW. Both the 12-fold symmetry and the self-similarity in two kinds of crystals will be helpful for the development of laser and optoelectronic integrated technique.

This work was supported by the National Natural Science Foundation of China (No. 11004175) and the Communication University of China (Science Planning Project).

References

1. J. A. Armstrong, N. Bloembergen, J. Ducuing, and P. S. Pershan, Phys. Rev. **127,** 1918 (1962).
2. Y. Y. Zhu, S. N. Zhu, and N. B. Ming, Science **278,** 843 (1997).
3. G. D. Miller, R. G. Batchko, W. M. Tulloch, D. R. Weise, M. M. Fejer, and R. L. Byer, Opt. Lett. **22,** 1834 (1997).
4. V. Berger, Phys. Rev. Lett. **81,** 4136 (1998).
5. B. Q. Ma, T. Wang, P. Y. Ni, B. Y. Cheng, and D. Z. Zhang, Europhys. Lett. **68,** 804 (2004).
6. K. Liu, J. H. Shi, and X. F. Chen, Appl. Phys. Lett. **94,** 101106 (2009).
7. K. Kalinowski, Q. Kong, V. Roppo, A. Arie, Y. Sheng, and W. Krolikowski, Appl. Phys. Lett. **99,** 181128 (2011).
8. D. Yudistira, S. Benchabane, D. Janner, and V. Pruneri1, Appl. Phys. Lett. **95,** 052901 (2009).
9. J. Burghoff, C. Grebing, S. Nolte, and A. Tünnermann, Appl. Phys. Lett. **89,** 081108 (2006).
10. M. Oxborrow and C. Henley, Phys. Rev. B **48,** 6966 (1993).